SEMARAK ILMU PUBLISHING

Journal of Advanced Research in Applied Sciences and Engineering Technology

https://semarakilmu.com.my/journals/index.php/applied_sciences_eng_tech/index
ISSN: 2462-1943

Bioheat transfer of Blood Flow on Healthy and Unhealthy Bifurcated Artery: Stenosis

Zuhaila Ismail[1,*], Muhammad Sabaruddin Ahmad Jamali[1], Norliza Mohd Zain[1], Lim Yeou Jiann[1]

[1] Department of Mathematical Sciences, Faculty of Science, Universiti Teknologi Malaysia, 81310 UTM Johor Bahru, Johor, Malaysia

ABSTRACT

The development and progression of stenosis with a high probability of rupture can be altered by changing the heat distribution in the bifurcated artery. The purpose of this study is to investigate the behavior of blood flow from healthy to unhealthy artery bifurcation under the influence of bioheat transfer. The blood flow is modelled as laminar, two-dimensional, steady, incompressible, and characterised as a Newtonian fluid. The Galerkin weighted residual (GWR) method is utilised to solve the governing equations. The behaviour of the blood flow due to different Reynolds numbers and the severity of stenosis is graphically investigated and discussed. The results reveal that the velocity profiles increase as the degrees of constriction increase. However, a lower Reynolds number enhances the axial velocity in an artery. The blood flow behaves differently from healthy to unhealthy on the bifurcated artery in the presence of an arterial constriction. The behaviour is significantly affected by the rate of heat transfer and the location of stenosis.

Keywords:
Bioheat transfer; bifurcated artery;
stenosis; Galerkin weighted residual

Received: 25 August 2022 **Revised: 2 October 2022** **Accepted: 4 October 2022** **Published: 17 October 2022**

1. Introduction

Atherosclerosis is one of the cardiovascular diseases that is notoriously known globally due to its morbidity rate. Atherosclerosis thickens and stiffens the arteries due to the built-up plaques in the inner lining of the artery. Over time, the plaque will block the bloodstream and reduce the oxygen supply to the vital organs as the plaque expands and ruptures. While the plaques keep on enlarging, stenosis is formed as the narrowing phenomenon occurred in the arteries. The existence of stenosis would impair the usual flow of blood through the artery, resulting in a reduction in the amount of blood carried to the desired site. Some of the atherosclerosis symptoms may cause heart problems since it can lead to stroke, heart attack, and blood clots [1].

Apart from that, an essential dynamics of blood flow factor that needs to be considered in current analyses is the arterial geometry. Studying the effect of these factors on the blood flow characteristics with heat transfer will help in a better understanding of the roles of blood dynamically

* *Corresponding author.*
E-mail address: zuhaila@utm.my

https://doi.org/10.37934/araset.28.2.5679

in the development and progression of arterial diseases. An initial investigation has been carried out so far on the blood flow problem that is recently focused on single stenosis in the artery and is assumed to be analytical due to some forms of certain mathematical functions. Therefore, Singh [2] investigated the effects of shape parameters and length of stenosis on blood flow through the improved generalized artery with multiple stenoses. Ledesma *et al*., [3] studied on experimentally based shape for the single stenotic artery in the presence of a catheter, where the blood was treated as a two-phase macroscopic model. Then, Riahi *et al*., [4] extended the study by assuming the blood flow in the presence of multi stenosis for the cases with or without a catheter. They discovered that the velocities are non-uniform at the constriction region and increase with the catheter radius. In reality, stenosis is usually formed irregularly and is found in the pulmonary and femoral arteries [5]. Therefore, predicting an appropriate shape of stenosis is very crucial. By considering the stenosis with an irregular shape related to the blood flow thus the problem would become more realistic [6]. Studies conducted by Zain *et al*., [1] and [7 - 17] have focused on the bifurcated artery with a stenosis, which is present at the mother artery or daughter artery itself. The authors in Zain *et al*., [1] and Zarins *et al*., Srinivasacharya *et al*., [10-11] also shared the same opinion as Rabby *et al*., [18], where they conclude that arterioles of regions with high curvatures or bifurcations and junctions occur where atherosclerotic lesions are mostly formed. The flow reversal and recirculation zones are formed downstream of stenosis and along the edge of the daughter artery [1]. It is believed that the existence of flow recirculation in the cardiovascular system can cause danger to the health of a person, especially atherosclerosis patients since the blood is moving slowly in this zone.

A considerable amount of work has been devoted to the study of heat transfer in the arterial system, and the blood flow problem concerning these parameters has been solved either analytically or numerically. It is worth mentioning that the study of heat transport phenomena inside the artery received much attention in recent times due to its wide applications in modern treatment, such as laser surgery, cryosurgery, hyperthermia, and hypothermia. An early attempt to study the convective impact of the bloodstream had been conducted by Friedman *et al*., [19]. They examined the two-dimensional bifurcated artery and found the results of an analytical boundary layer in the mass concentration inside an arterial wall. The author in Ogulu and Tamunoimi [20] conducted the study of heat transfer simulation on oscillatory blood flow in an indented porous artery. They assume the artery with mild stenosis that incorporate radiative heat transfer and the presence of a uniform magnetic field. The study of the dynamic response of heat and mass transfer in the blood flow through a stenosed bifurcated artery was conducted by Friedman *et al*., [19]. They considered blood as a Newtonian fluid, and the finite difference method has been used to solve the equations.

Li *et al.,* [21] studied heat transfer on a steady spatially varying magnetic field and implemented the numerical finite volume method to solve the problem. They concluded that the field of the flow and temperature are affected by the field of magnetic. Investigation of the catheterized artery was done by Srikanth *et al*., [22] by assuming velocity slip through the tapered w-shape stenosed artery. The effects of heat and mass transfer on blood flow through a tapered artery with overlapping stenosis were analyzed by Zaman *et al*., [23]. Numerical research of heat transfer in a stenosed arterial segment concerning MHD flow of blood was presented by Majee *et al*., [24]. The dissipation of energy was taken into consideration due to the application of the magnetic field in streaming blood. It is interesting to note that the mentioned studies above are recently conducted within a single channel of the artery. Recently, the simulation of heat transfer on blood flow through a stenosed bifurcated artery was presented by Jamali *et al*., [14]. They concluded that the backflow occurs, and recirculation zones were formed where the corresponding region dominated by arterial wall temperature itself might expose an individual to a worsening effect of cardiovascular diseases.

Thus, bioheat transfer is one of the important parameters that need to be considered in blood flow investigation.

Various methods can be used to solve the problem of blood flow in the stenosed artery, as the study of mathematical variables can help the researcher to get a clear understanding of a more approximate result. Two ways of mathematical study can be performed are analytical and numerical approaches. However, due to the complexity of the models, solving them analytically will be very difficult. The introduction of numerical methods, so far, is used widely because of its simpler and convenience through experimental or theoretical in different scientific interests. The study of blood flow modeling by Bessonov *et al*., [25] concluded that there are diverse methods for numerical solutions. They started the incomplete list containing Taylor-Galerkin methods and discontinuous Galerkin, second-order local conservative Galerkin method, least-square method, high-order finite volume method, finite differences with artificial viscosity method, and characteristic methods. Enormous recent and previous studies on blood flow in a stenosed artery were reported to be solved by numerical methods [1] and [27-31]. The finite difference method based on the central difference approximation has been employed by [26,30]. Meanwhile, the blood motion using the Crank-Nicolson implicit finite difference method was used by Misra and Pal [31]. Furthermore, Abdullah *et al.,* [28] conducted a study on blood flow through a tapered overlapping stenosed artery using the finite difference method.

Besides the numerical methods that have been reviewed above, the finite element method (FEM) was utilized in the research on arterial blood flow either in two-dimension or three-dimension problems. The finite element term was initially introduced by Clough [32] in the study of plane elasticity and is one of the well-established methods that can be used as a powerful tool to solve complex problems of differential equations that describe different physical processes. The advantage of FEM is its ability to deal with irregular shape boundaries. FEM also provides a faster rate of convergence [33]. Not limited only to the structural field, FEM also has the advantage of applying to domains with complex geometry. The author in Yashkun *et al*., [34] studied the steady-state flow of blood in the bifurcated artery by considering the blood as a generalized Newtonian fluid. Simulation is performed by implementing the Galerkin weighted residual (GWR) as a method of solution. The author in Achaba *et al*., [35] investigated the periodic blood flow through a stenotic artery by considering the Cross model and generalized power law as the shear-thinning characteristic.

As far as the author's knowledge, there is a limited study in the literature on the blood flow with bioheat in a bifurcated artery under influence of different types of stenosis. The novelty of this present paper is to simulate the influence of bioheat transfer on blood flow through healthy (without stenosis) and unhealthy (with stenosis) bifurcated arteries by using the Galerkin weighted residual (GWR) method via MATLAB. The influence of the bioheat transmission may cause an irreversible effect on the protein contained in the blood which may lead to fatality death. The unnatural growth that happens in the bifurcated artery called stenosis, gives a significant effect on the blood flow and thermal characteristics in the artery. Therefore, the present study aims to investigate the streaming of blood with bioheat transfer through a bifurcated channel without and with different types of stenosis. The blood flow is assumed to be steady, incompressible, laminar, and fully developed. The effect of the bioheat transfer on the streaming of the blood is observed and analyzed. The implementation of the GWR in MATLAB to compute and visualize the numerical solutions is discussed. The profiles and contour of the blood flow in the bifurcated artery under the impact of bioheat transfer for different Reynolds numbers and the severity of stenosis are presented and discussed.

2. Mathematical Formulation

Four different types of stenosis in bifurcated artery with the effect of heat transfer is presented. In order to formulate the computational domain for the stenosed bifurcated artery, these following assumptions are imposed: The artery forming bifurcation is of finite length; 4 possible morphologies considered from TYPE I to TYPE IV, as shown in Figure 1; Curvatures are introduced at the lateral junctions and the flow divider of the arterial bifurcation to ensure that one can rule out the presence of any discontinuity causing non-existent of separation zones. Generally, stenosis does not have a fix shape. In fact, its shape is usually irregular. Four different types of stenosis have been proposed and used to define these lesions, as shown in Figure 1. TYPE I is no stenosis in bifurcated artery and it is considered as healthy bifurcated artery. TYPE II, stenosis involves in the parent artery proximal to bifurcation. TYPE III, stenosis located in the parent artery elongate into upper wall of bifurcation. TYPE IV, stenosis located in the parent vessel, proximal and ostium of bifurcation. The idea to proposed these four different types of stenosis in a bifurcated artery from healthy to unhealthy bifurcated artery is come from [5].

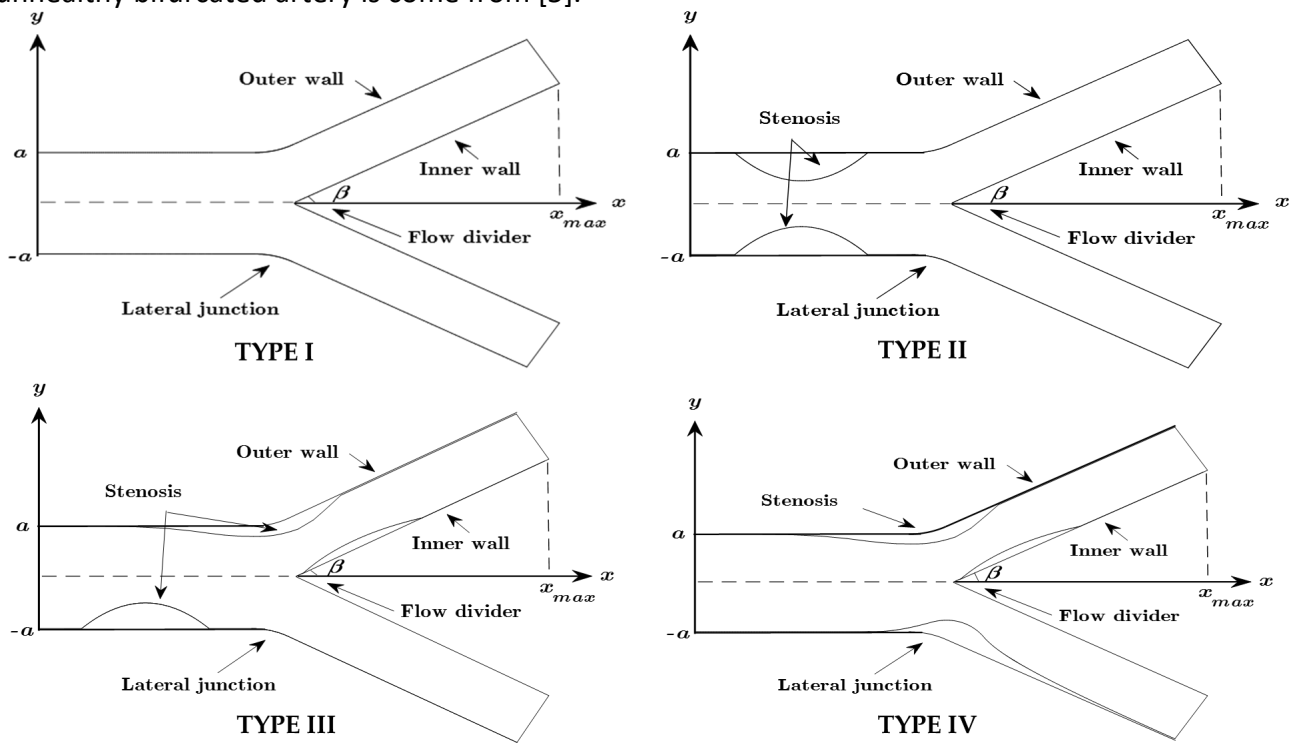

Fig. 1. Four different location of stenosis that will be considered in this study

2.1 Governing Equations

The governing equations with heat transfer, in dimensionless form, can be written as

$$\frac{\partial u}{\partial x}+\frac{\partial v}{\partial y}=0, \tag{1}$$

$$u\frac{\partial u}{\partial x}+v\frac{\partial u}{\partial y}=-\frac{\partial p}{\partial x}+\frac{1}{\mathrm{Re}}\left(\frac{\partial^2 u}{\partial x^2}+\frac{\partial^2 u}{\partial y^2}\right), \tag{2}$$

$$u\frac{\partial v}{\partial x}+v\frac{\partial v}{\partial y}=-\frac{\partial p}{\partial y}+\frac{1}{\mathrm{Re}}\left(\frac{\partial^2 v}{\partial x^2}+\frac{\partial^2 v}{\partial y^2}\right), \tag{3}$$

$$u\frac{\partial T}{\partial x}+v\frac{\partial T}{\partial y}=\frac{1}{\mathrm{Re}\,\mathrm{Pr}}\left(\frac{\partial^2 T}{\partial x^2}+\frac{\partial^2 T}{\partial y^2}\right) \tag{4}$$

where $\mathrm{Re}=\rho L U_0/\mu$ and is named as Reynolds number. $\mathrm{Pr}=\mu c_p/k$, named as Prandtl number (dimensionless number represents the ratio of molecular diffusivity of the momentum to the molecular diffusivity of the heat).

2.2 Boundary Conditions

At the inlet, a parabolic velocity profile is assumed to be a fully developed flow with constant temperature given by

$$u(x,y)=u_{\max}\left(1-\frac{y^2}{a^2}\right) \text{ and } v(x,y)=0,\ T_{in}=1, \text{at } x=0 \text{ and } -a\le y\le a. \tag{5}$$

Moreover, a uniform temperature is assumed to be zero at the wall of artery, $T_{wall}=0$. Along all the arterial walls, the usual no-slip conditions are prescribed as

$$u(x,y)=0,\ v(x,y)=0. \tag{6}$$

At the outlets, a traction-free condition is applied which can be stated as

$$\left(-p\mathbf{I}+\tau\right)\cdot\mathbf{n}=0, \tag{7}$$

where $\mathbf{n}$ represents a unit outward normal vector with the pressure point constraint, $p=0$ being implemented at $x=0$ and $y=-0.5$.

3. Galerkin Weighted Residual Method

The governing equations given in Eq. (1) – Eq. (4) need to discretize by employing the Galerkin weighted residual (GWR) method. In each finite element $e_i, i=1,2,\ldots n,$ the variables $(u^{e_i},\ v^{e_i},\ T^{e_i},\ P^{e_i})$ are approximated as

$$\begin{aligned}
u&=u^{e_i}=\delta_j^{e_i}(x,y)\,u_j^{e_i},\ j=1,2,\ldots,6,\\
v&=v^{e_i}=\delta_j^{e_i}(x,y)\,v_j^{e_i},\ j=1,2,\ldots,6,\\
P&=P^{e_i}=\psi_k^{e_i}(x,y)\,P_k^{e_i},\ k=1,2,3,\\
T&=T^{e_i}=\delta_j^{e_i}(x,y)\,T_j^{e_i},\ j=1,2,\ldots,6.
\end{aligned} \tag{8}$$

$\delta_j^{e_i}$ and $\psi_k^{e_i}$ in Eq. [8] are the shape functions for the dependent variables' velocity, temperature and the pressure respectively. GWR method is practiced in this study. After discretises the Eq. (1) by the method, the Eq. (1) can be represented in a matrix form as

$$\begin{bmatrix} D_{11} & D_{12} & D_{13} & D_{14}\\ D_{21} & D_{22} & D_{23} & D_{24}\\ D_{31} & D_{32} & D_{33} & D_{34}\\ D_{41} & D_{42} & D_{43} & D_{44}\end{bmatrix}\begin{Bmatrix} E_1\\ E_2\\ E_3\\ E_4\end{Bmatrix}=\begin{bmatrix} F_1\\ F_2\\ F_3\\ F_4\end{bmatrix}, \tag{9}$$

where

$$D_{11}=\left[\int_{A_{e_i}}\left\{\delta_l^{e_i}\right\}\left(u^{e_i}\frac{\partial\left\{\delta_j^{e_i}\right\}}{\partial x}+v^{e_i}\frac{\partial\left\{\delta_j^{e_i}\right\}}{\partial y}\right)+\frac{1}{\mathrm{Re}}\left(\frac{\partial\left\{\delta_l^{e_i}\right\}}{\partial x}\frac{\partial\left\{\delta_j^{e_i}\right\}}{\partial x}+\frac{\partial\left\{\delta_l^{e_i}\right\}}{\partial y}\frac{\partial\left\{\delta_j^{e_i}\right\}}{\partial y}\right)dA_{e_i}\right],\ D_{13}=\left[\int_{A_{e_i}}\left\{\delta_l^{e_i}\right\}\frac{\partial\left\{\psi_k^{e_i}\right\}}{\partial x}dA_{e_i}\right],$$

$$D_{23}=\left[\int_{A_{e_i}}\left\{\delta_l^{e_i}\right\}\frac{\partial\left\{\psi_k^{e_i}\right\}}{\partial y}dA_{e_i}\right],\ D_{31}=\left[\int_{A_{e_i}}\left\{\psi_m^{e_i}\right\}\frac{\partial\left\{\delta_j^{e_i}\right\}}{\partial x}dA_{e_i}\right],\ D_{32}=\left[\int_{A_{e_i}}\left\{\psi_m^{e_i}\right\}\frac{\partial\left\{\delta_j^{e_i}\right\}}{\partial y}dA_{e_i}\right],$$

$$D_{44}=\left[\int_{A_{e_i}}\left\{\delta_l^{e_i}\right\}\left(u^{e_i}\frac{\partial\left\{\delta_j^{e_i}\right\}}{\partial x}+v^{e_i}\frac{\partial\left\{\delta_j^{e_i}\right\}}{\partial y}\right)+\frac{1}{\mathrm{Re\,Pr}}\left(\frac{\partial\left\{\delta_l^{e_i}\right\}}{\partial x}\frac{\partial\left\{\delta_j^{e_i}\right\}}{\partial x}+\frac{\partial\left\{\delta_l^{e_i}\right\}}{\partial y}\frac{\partial\left\{\delta_j^{e_i}\right\}}{\partial y}\right)dA_{e_i}\right],D_{12}=D_{21}=D_{41}=D_{14}=D_{24}=D_{42}=\left[0\right]_{6\times6},$$

$$D_{33}=\left[0\right]_{3\times3},D_{34}=\left[0\right]_{3\times6},\ D_{43}=\left[0\right]_{6\times3},\ D_{22}=D_{11},$$

$$F_1=\int_{\Gamma_{e_i}}\frac{1}{\mathrm{Re}}\left(\left\{\delta_l^{e_i}\right\}\frac{\partial\phi_j^{e_i}u_j^{e_i}}{\partial x}n_x+\left\{\delta_l^{e_i}\right\}\frac{\partial\phi_j^{e_i}u_j^{e_i}}{\partial y}n_y\right)d\Gamma_{e_i},$$

$$F_2=\int_{\Gamma_{e_i}}\frac{1}{\mathrm{Re}}\left(\left\{\delta_l^{e_i}\right\}\frac{\partial\delta_j^{e_i}v_j^{e_i}}{\partial x}n_x+\left\{\delta_l^{e_i}\right\}\frac{\partial\delta_j^{e_i}v_j^{e_i}}{\partial y}n_y\right)d\Gamma_{e_i},$$

$$F_3=\left[0\right]_{3\times1},\ F_4=\int_{\Gamma_{e_i}}\frac{1}{\mathrm{Re\,Pr}}\left(\left\{\delta_l^{e_i}\right\}\frac{\partial\delta_j^{e_i}T_j^{e_i}}{\partial x}n_x+\left\{\delta_l^{e_i}\right\}\frac{\partial\delta_j^{e_i}T_j^{e_i}}{\partial y}n_y\right)d\Gamma_{e_i}.$$

$$E_1=\left\{u_j^{e_i}\right\}^T,\ E_2=\left\{v_j^{e_i}\right\}^T,\ E_3=\left\{P_k^{e_i}\right\}^T,E_4=\left\{T_j^{e_i}\right\}^T,$$

$$\left\{u_j^{e_i}\right\}^T=\left\{u_1^{e_i}\quad u_2^{e_i}\quad u_3^{e_i}\quad u_4^{e_i}\quad u_5^{e_i}\quad u_6^{e_i}\right\}^T,$$

$$\left\{v_j^{e_i}\right\}^T=\left\{v_1^{e_i}\quad v_2^{e_i}\quad v_3^{e_i}\quad v_4^{e_i}\quad v_5^{e_i}\quad v_6^{e_i}\right\}^T,$$

$$\left\{T_j^{e_i}\right\}^T=\left\{T_1^{e_i}\quad T_2^{e_i}\quad T_3^{e_i}\quad T_4^{e_i}\quad T_5^{e_i}\quad T_6^{e_i}\right\}^T,$$

$$\left\{P_k^{e_i}\right\}^T=\left\{P_1^{e_i}\quad P_2^{e_i}\quad P_3^{e_i}\right\}^T,\left\{\delta_l^{e_i}\right\}=\left\{\delta_j^{e_i}\right\}^T,\left\{\psi_m^{e_i}\right\}=\left\{\psi_k^{e_i}\right\}^T$$

$$\left\{\delta_j^{e_i}\right\}=\left\{\delta_1^{e_i}\quad\delta_2^{e_i}\quad\delta_3^{e_i}\quad\delta_4^{e_i}\quad\delta_5^{e_i}\quad\delta_6^{e_i}\right\},\left\{\psi_k^{e_i}\right\}=\left\{\psi_1^{e_i}\quad\psi_2^{e_i}\quad\psi_3^{e_i}\right\}.$$

Assemble the element matrix (9) for each finite element into a global matrix and then determine the solutions by solving the global matrix with subjecting to the boundary conditions (given in Eq. (5) – Eq. (7)). Nevertheless, the global matrix is a nonlinear system since Eq. (9) is nonlinear, thus it is needed to solve the system in an iteration manner. Newton-Raphson methods is applied to solve the global nonlinear system.

4. MATLAB Code Validation

MATLAB was used to create the GWR formulation source code. The sourcecode was checked for reliability and appropriate operation using the model proposed by Srinivasacharya *et al*., [11]. Then, the mesh test dependency test is carried out for the current problem in making sure that the numerical results is not depend on the mesh parameters.

4.1 Validation

Model validation is performed to convince that the source code developed using MATLAB software is properly programmed according to the GWR algorithm. Therefore, in order to have a thorough quantitative analysis of GWR onto the stenotic bifurcated artery flow phenomenon, constructed geometry, as shown in Figure 2 and parameter values employed based on model proposed by Srinivasacharya *et al*., [11] where

$a = 0.0075\text{m},\ l_0 = 0.015\text{m},\ d = 0.005\text{m},\ x_{\max} = 0.06\text{m},\ x_1 = 0.025\text{m},\ \mu = 0.0035\text{kgm}^{-1}\text{s}^{-1},$
$\rho = 1050\text{kgm}^{-3},\ \beta = 30^{\circ},\ q = 0.002\text{m},\ r_1 = 0.51a.$

$$R_1(x) = \begin{cases} a, 0 \le x \le d,\ d + l_0 \le x \le x_1, \\ a - \dfrac{4\tau_m}{l_0^2}\left(l_0(x-d) - (x-d)^2\right), d \le x \le d + l_0, \\ a + r_0 - \sqrt{r_0^2 - (x - x_1)^2},\ x_1 \le x \le x_2, \\ 2r_1 \sec\beta + (x - x_2)\tan\beta,\ x_2 \le x \le x_{\max} - s, \end{cases} \text{ and } \quad R_2(x) = \begin{cases} 0, & 0 \le x \le x_3, \\ \sqrt{r_0^{'} - \left(x - \left(x_3 + r_0^{'}\right)\right)^2}, & x_3 \le x \le x_4, \\ r_0^{'}\cos\beta + \left(x - x_4\right)\tan\beta, & x_4 \le x \le x_{\max}, \end{cases} \quad (10)$$

where $R_1(x)$ and $R_2(x)$ represent the radii of the outer and inner wall, respectively. Meanwhile, a and r_1 are the respective radii of the mother and daughter artery. r_0 and $r_0^{'}$ are the radii of curvature for the lateral junction and the flow divider, respectively. Whereas, l_0 is the length of the stenosis at a distance d from the origin. Location of the onset and offset of the lateral junction are denoted by x_1 and x_2 respectively. x_3 indicated as the apex, τ_m represents the maximum height of stenosis occur at $d + l_0/6$ and $d + 5l_0/6$ while β denote half of the bifurcation angle. Parameters involved in the above expressions may be given as

$x_2 = x_1 + r_0\sin\beta,\ r_0 = (a - 2r_1\sec\beta)/(\cos\beta - 1),\ r_0^{'} = \left(x_3 - x_2\right)\sin\beta/1 - \sin\beta,\ x_3 = x_2 + q,\ s = 2r_1\sin\beta,$
$x_4 = x_3 + r_0^{'}\left(1 - \sin\beta\right).$

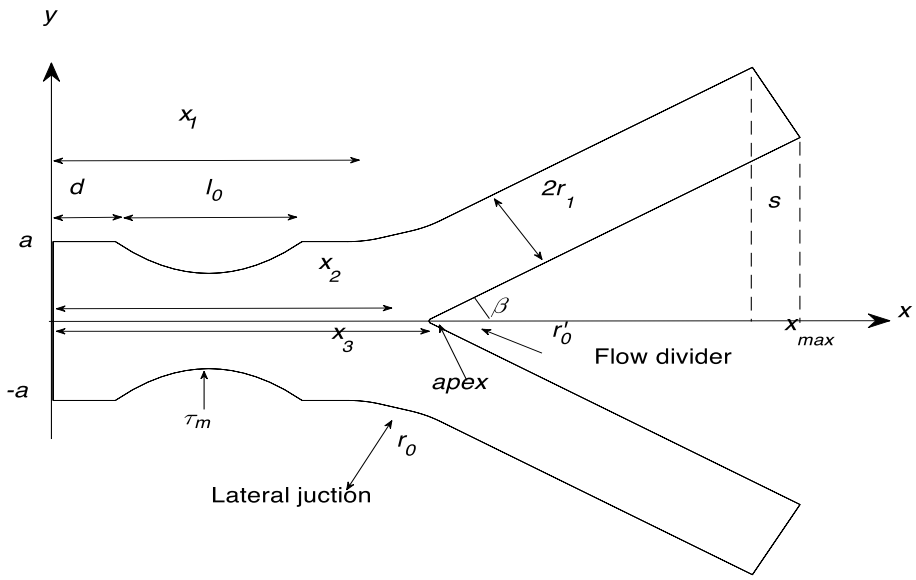

Fig. 2. Geometry of the stenosed arterial bifurcation model based on the Eq. (10), refer [11]

A personal computer with a processor speed of 2.30 [GHz] and a RAM of 8 [GB] was used to compute all the numerical results in this chapter. The same procedure of mesh is conducted with four different attempts of meshes. The best mesh generated by mesh2d displayed in Figure 3 by generate 10329 elements, 21004 nodes and 68350 DOFs. Thus, the global element matrix and global tangent matrix constructed with dimensions of 68350 x 68350. The domain was meshed and evaluated with solutions found converged at $\tau = 0.0001$. Figure 4 is velocity profile at the maximum constriction region of stenosis $x = 0.0125m$. The Table 1 shows that the results from those literature and COMSOL are in excellent match between each other.

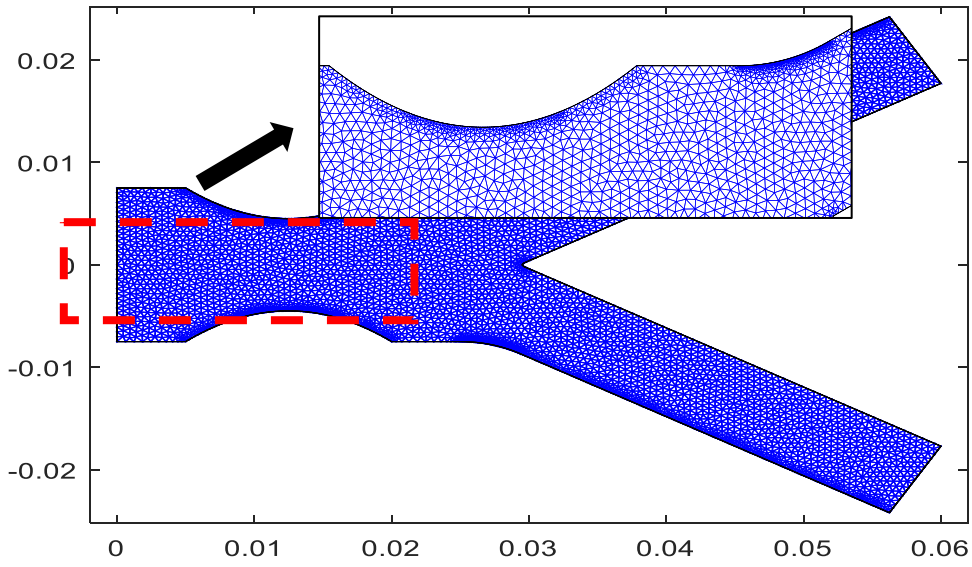

Fig. 3. Triangular mesh for stenosed bifurcated artery problem

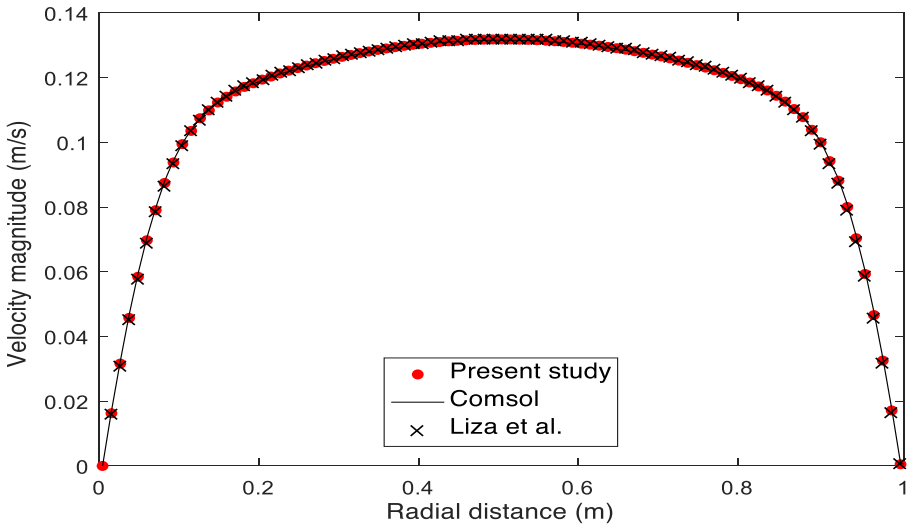

Fig. 4. Velocity profile at the maximum constriction region of stenosis $x = 0.0125m$

Table 1
Comparison of numerical results of maximum velocity and their coordinate

Authors	Maximum velocity	Coordinate (x,y)
Present	0.1345	$(0.1498, -5.6418\times10^{-5})$
COMSOL Multiphysics 5.2	0.1345	$(0.1499, -8.948\times10^{-5})$
Zain (2017)	0.1346	$(0.1500, -2.6418\times10^{-5})$

4.2 Mesh Dependency Test

The best mesh selected for all TYPE, refer Figure 5. Table 2 shows the summary of parameters for different mesh for all interest domain. The same procedure of meshing is applied to four different types of the arterial bifurcation (TYPE I, TYPE II, TYPE III, TYPE IV) by considering blood as Newtonian and Re=300. Several trials of mesh have been made for all type of geometry and only the stable mesh of them is selected and mentioned here, as shown in Figure 4. In order to get an excellent solution, the total number of elements between 11000-13000 are used to mesh the domain with the total number 6000-8000 nodes that generated the degree of freedom around 19000-23000 thus producing the global Jacobian and stiffness matrix of size 19000x 23000.

Table 2
Mesh parameters computed in COMSOL Multiphysics and MATLAB

Type of bifurcated artery	Domain elements	Maximum velocity	Coordinate (x,y)
TYPE I	22739	0.8089	(0.000,0.000)
TYPE II	23420	2.0149	(0.9936,-0.0014)
TYPE III	23420	1.9596	(2.3048,0.3742)
TYPE IV	24143	2.2823	(2.3224,0.3301)

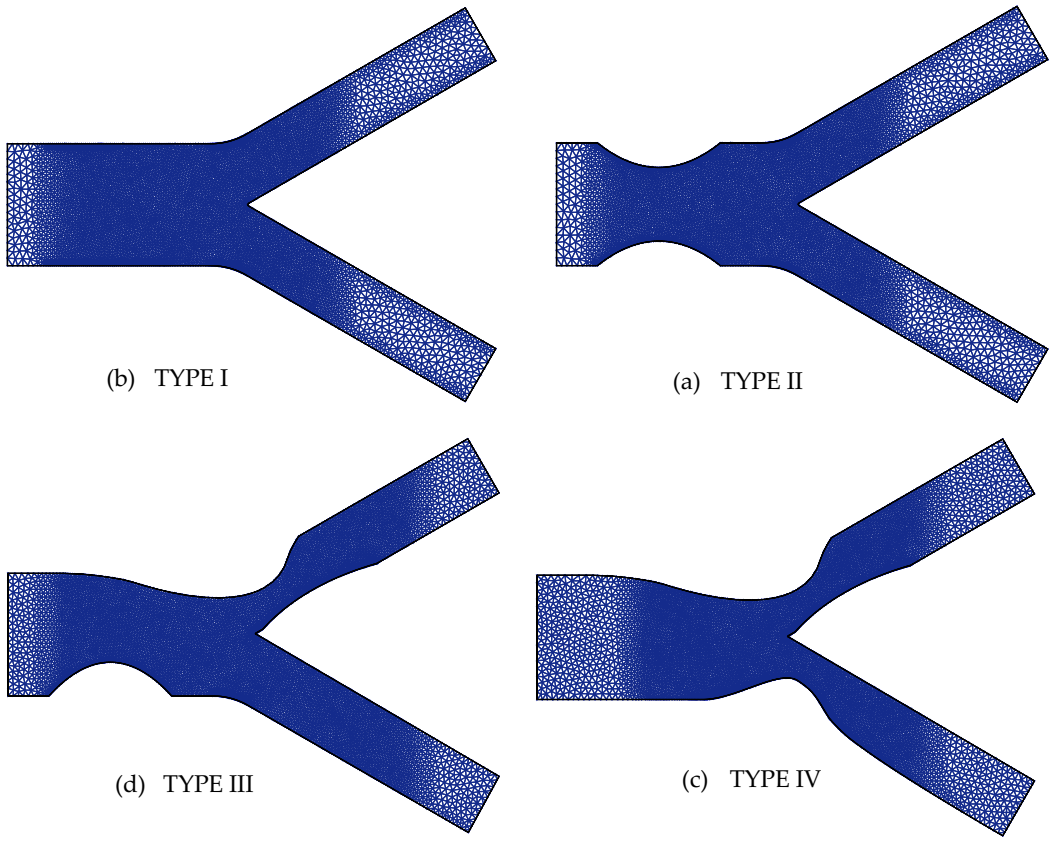

Fig. 5. Generated unstructured triangular meshes for all type of geometry

5. Results and Discussion

The constriction of the blockage or known as the throat determines the occlusion. A1 and A2 are the positive constants that control the maximum height of stenosis for geometry TYPE II, TYPE III, and TYPE IV, respectively. In this study, TYPE I is the control sample, so do not have the constriction value. Table 3 shows the summary for the values of constriction degree.

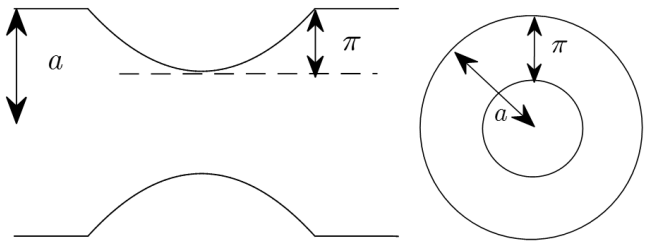

Fig. 6. The geometry showing the maximum height of stenosis

Table 3
Value of constriction degree for all of model geometry

Location of Stenosis	Maximum Height of Stenosis		Wall of Artery
	A1	A2	
TYPE I	0	0	Upper and lower wall Mother artery
TYPE II	0.2	0.25	Upper and lower wall Mother artery
TYPE III	0.2	0.25	Lower wall mother artery
	0.19	0.24	Upper wall lateral junction
TYPE IV	0.21	0.26	Lower wall lateral junction
	0.19	0.24	Upper wall lateral junction

5.1 Velocity Profile

Figures 7 – 9 show the velocity contour plot for TYPE II-IV corresponding to several parameters, respectively. The role of the maximum height of stenosis and Reynold number on the velocity profile are presented. The velocity gradient for different Reynold numbers and the maximum height of stenosis are plotted. The arrow in the figures shows the direction of the blood flow in the artery. Overall, the maximum velocity has a positive function with the maximum height of stenosis, whereas a reverse relationship is observed in Figures 6-8 for the Reynold number.

In TYPE II, the maximum velocity is formed nearby the bifurcate downstream of the throat of stenosis. In TYPE III and IV, the maximum velocity happens at the throat of stenosis in the bifurcation part. The height of stenosis may decelerate the flow of blood inside the bifurcated artery. Noteworthy, the maximum velocity in TYPE III is in the bifurcate throat, though the maximum height of stenosis happens at the mother artery part. This is contributed by the narrowing and small range of the artery radius. Furthermore, TYPE IV shows the highest value of maximum velocity compared to other TYPE due to the minor stenosis which allows much blood flow through the divider. The presence of plaque deposition in the bifurcated artery may reduce the supply of blood to the organs. If the stenosis continues to enlarge, an individual may suffer from cardiovascular disease.

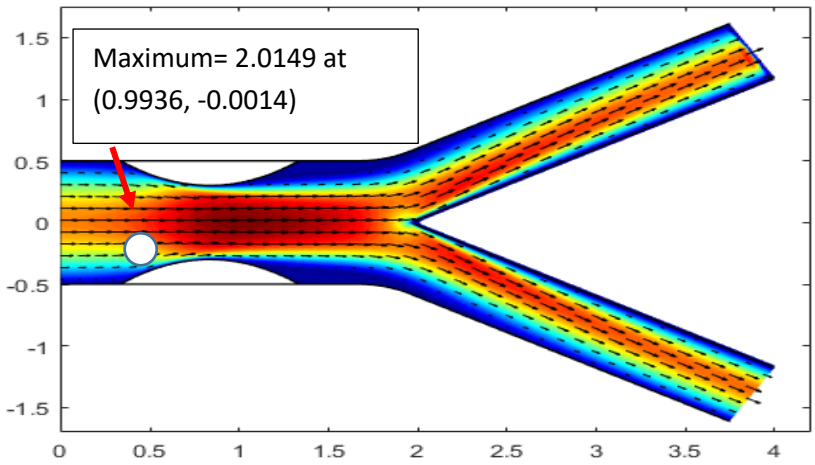

(a) Re=300, A1

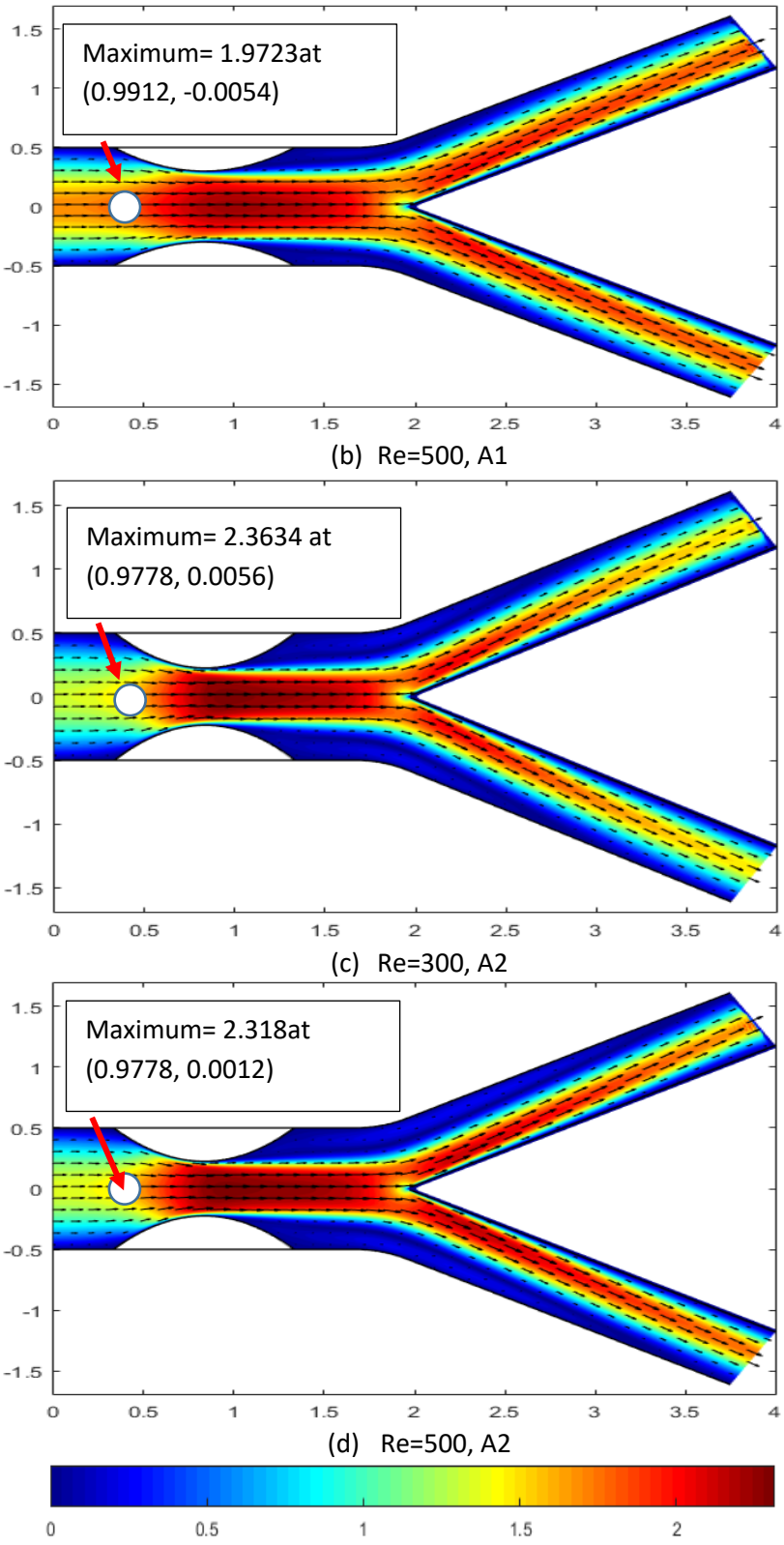

Fig. 7. Velocity contour for TYPE II with different Reynold number, 300 and 500, and maximum height of stenosis, A1 and A2

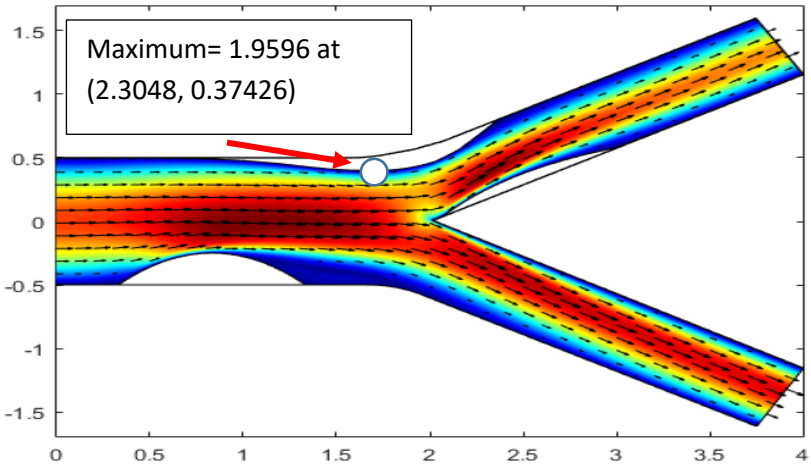

(a) Re=300, A1

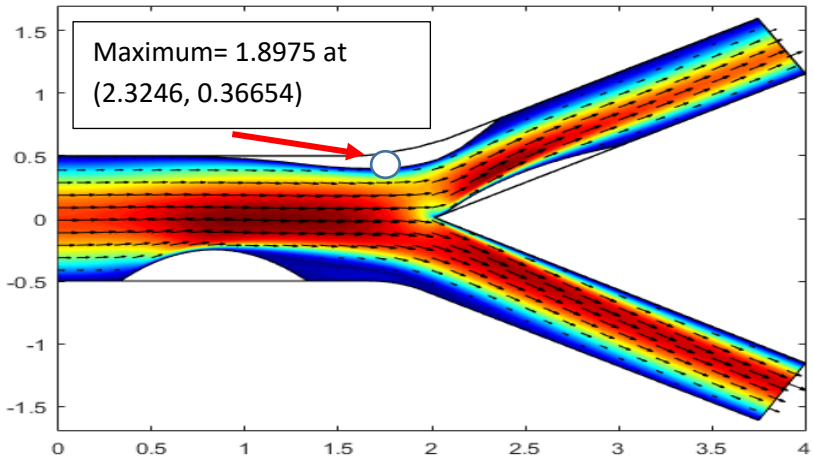

(b) Re=500, A1

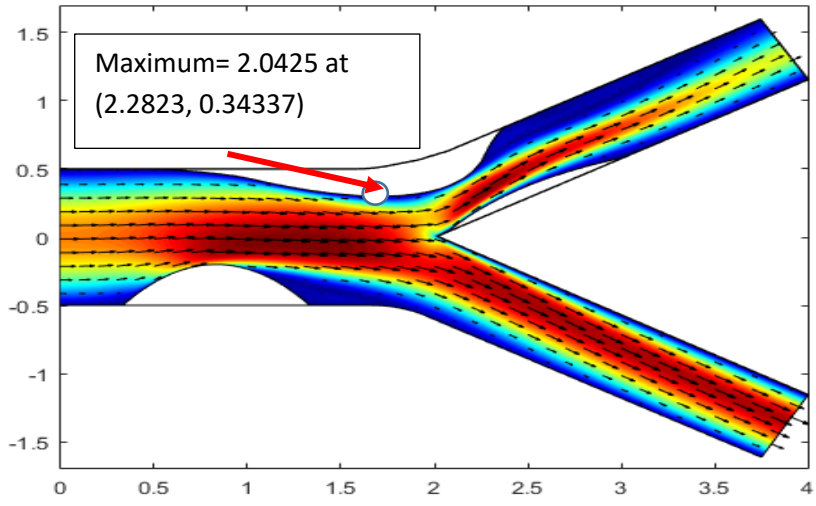

(c) Re=300, A2

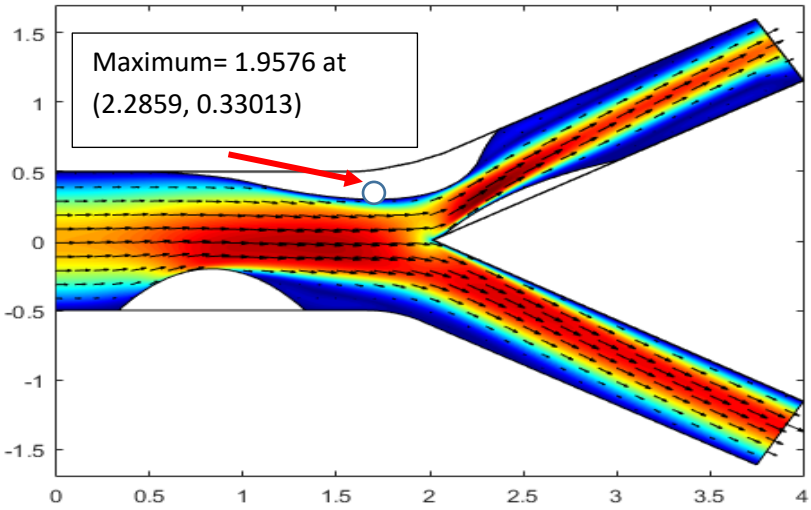

(d) Re=500, A2

Fig. 8. Velocity contour for TYPE III with different Reynold number, 300 and 500, and maximum height of stenosis, A1 and A2

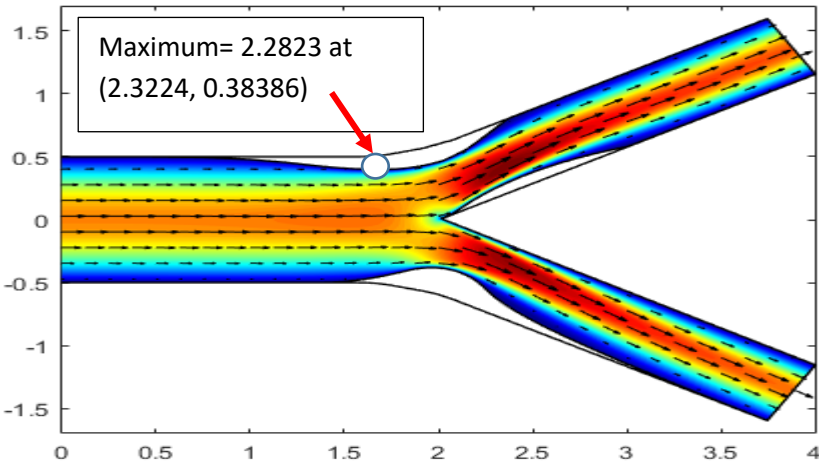

(a) Re=300, A1

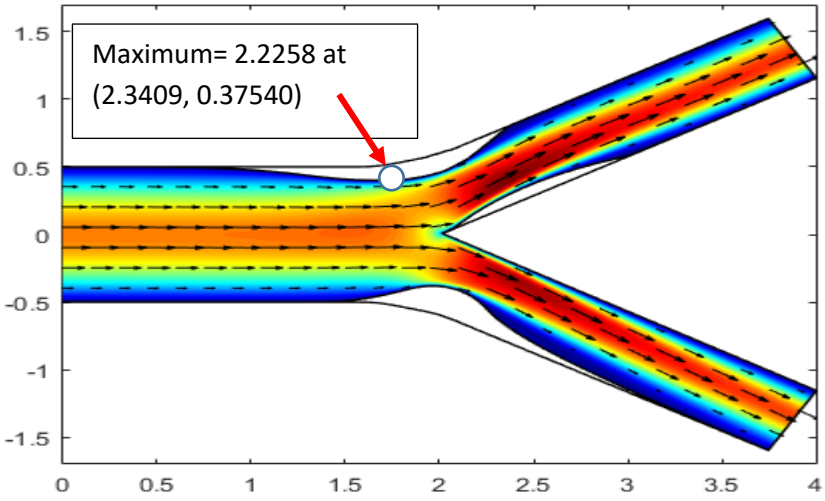

(b) Re=500, A1

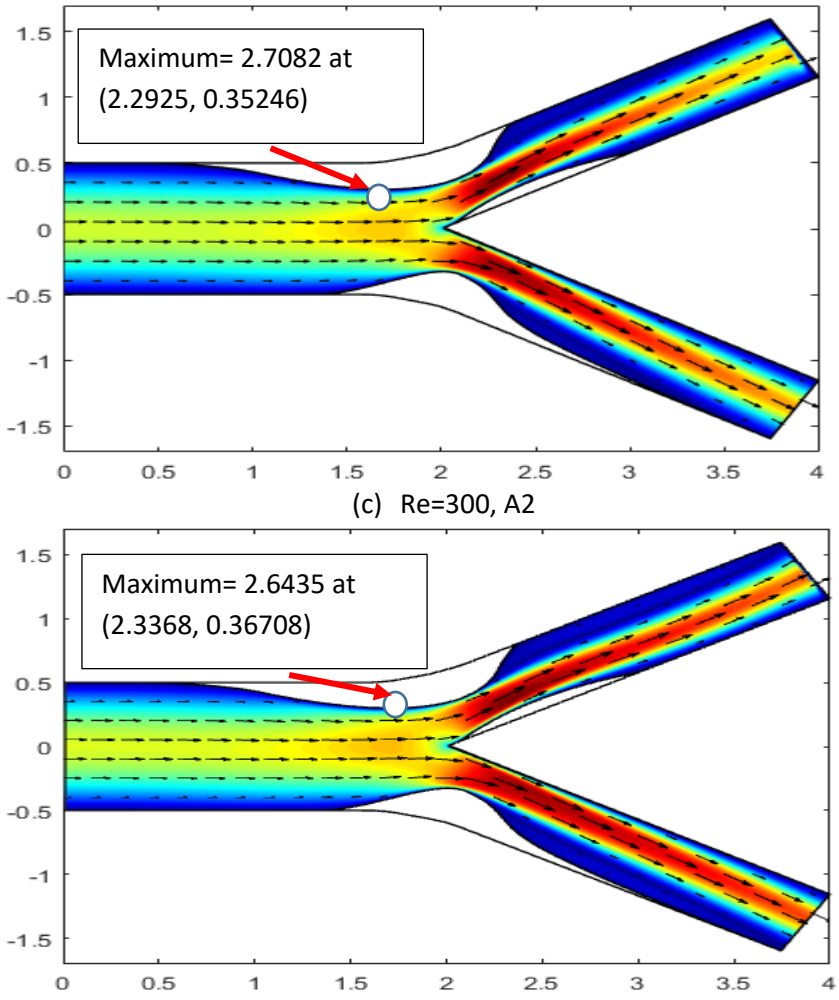

(c) Re=300, A2

(d) Re=500, A2

Fig. 9. Velocity contour for TYPE IV with different Reynold number, 300 and 500, and maximum height of stenosis, A1 and A2

Figures 10 (a) – 10 (d) illustrate the cross-sectional axial velocity profiles corresponding to different axial positions in the bifurcated artery with various maximum heights of stenosis, and Reynold number, respectively. The velocity of the blood flow reaches maximum value along the centreline of the artery as seen in Figures 10 (a) – 10 (d). Since the vessel is assumed to obey the non-slip condition and behaves like a rigid wall. Thus, the maximum value drops gradually to zero as approaches the vessel wall.

Figure 10 (a) shows the velocity profile of TYPE II at $x = 0.85$, which is located right on the maximum height of stenosis. The narrowing of the artery has significantly increased the velocity profile. The role of the Reynold number for each maximum height of stenosis A1 and A2, respectively, on the velocity profile, is presented. As the Reynold number increases, the profile curve behaves in a flattening shape compared to the lower Reynold number. This has caused the blood to move slowly along the axial direction near the central axis of the vessel. This finding is well supported by Srinivasacharya *et al*., [11].

The velocity profile nearby to the central passage of the bifurcated artery at $x = 1.35$ of TYPE II is shown in Figure 10 (b). Here, the normal artery (TYPE I) has been applied to compare the velocity profile at the same evaluation location. For Re=300 and the maximum height of stenosis of A2, the blood move with the highest value of velocity as compared to TYPE I with Re=300. A normal parabolic

velocity profile is seen for the artery without stenosis. Interestingly, near the wall surface, the fluid velocity decreases to a negative value and then increases back to zero. This is because of the occurrence of backflow and arising of separation flow. This phenomenon has been observed by Zain *et al*., [12]. Zarins *et al*., [10] suggested that the development of platelet deposition was significantly trigged by the appearance of separation flow and then lead to the complication of intimal thickening formation.

The axial velocity profile of TYPE II at the apex $x = 2$ and the daughter branch $x = 2.75$ are plotted in Figure 10 (c) and Figure 10(d) respectively. The blood exhibits the highest velocity with Re=500 and stenosis A2. The largest negative flow has also formed. The occurrence of reversal flow as depicted in Figure 10 (b) for (Re=300, A1) is now fully overcome at $x = 2$. Since no negative flow developed at this region except for (Re=300, A2), (Re=500, A1) and (Re=500, A2). Figure 10 (d) shows that the parabolic velocity profile is divided into two parts regarding the physical shape of a bifurcation. The upper and lower branch of the bifurcation artery. The velocity profile for the upper branch is skewed to the right and the left for the lower branch. A reversal flow is developed in the post-stenotic region near the outer wall surface. This has influenced the surrounding blood flow by pushing it toward the inner wall of the daughter branch. The blood flow profile for TYPE I and II with Re=300 and Re=500 are compared. As seen, the formation of the stenosis gives a significant effect on the velocity of the streaming blood.

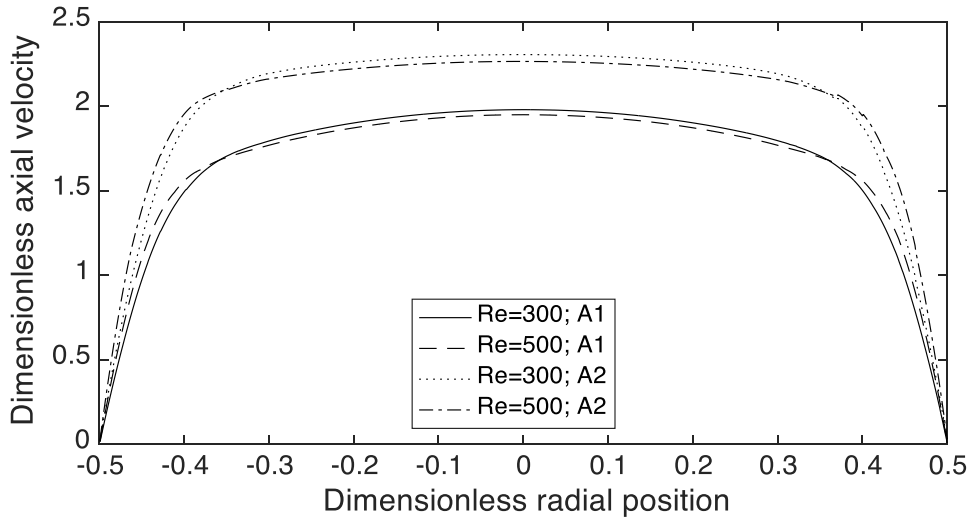

(a) TYPE II at $x = 0.85$

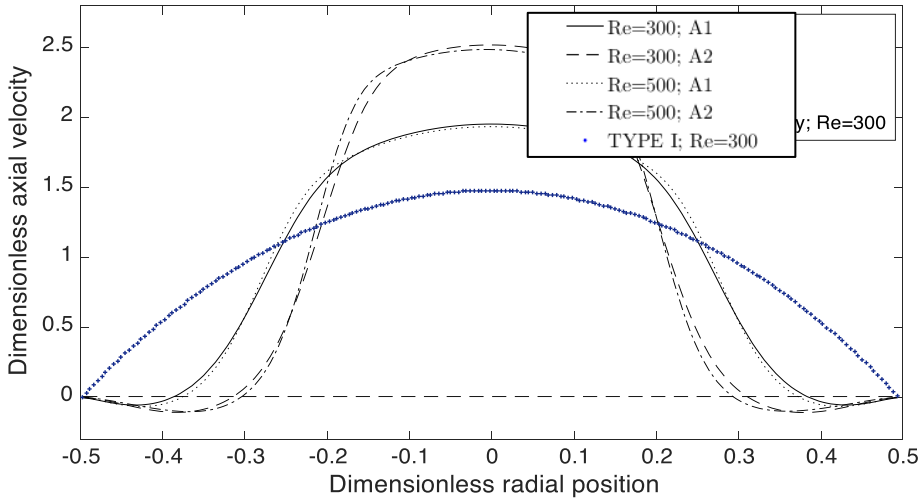

(b) TYPE II at $x = 1.35$

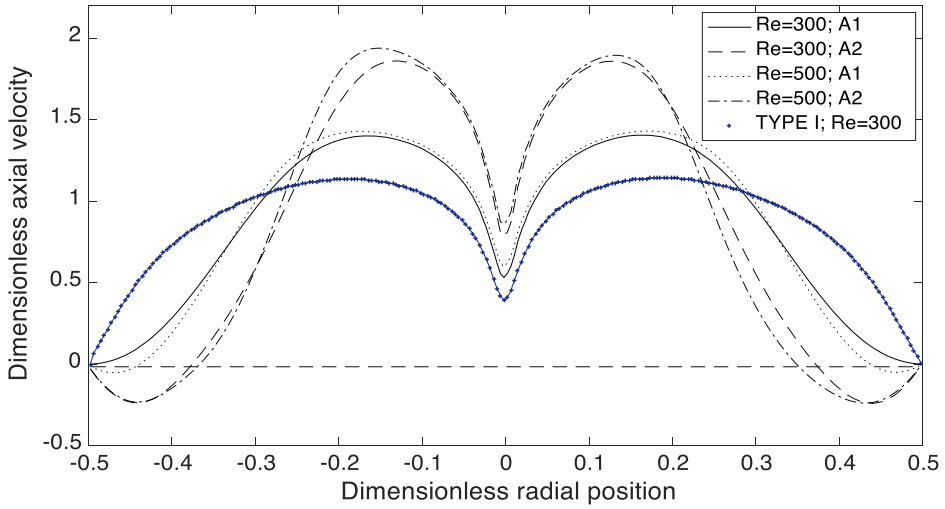

(c) TYPE II at $x = 2$

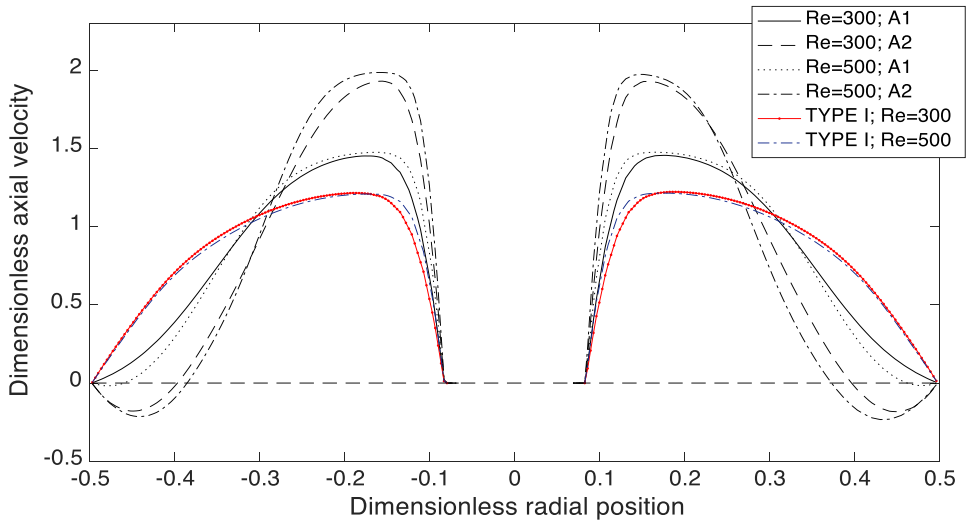

(d) TYPE II at $x = 2.75$

Fig. 10. Velocity profile with different Reynold number (300 and 500), at different value of *x* and maximum height of stenosis

Figure 11 depicts the dimensionless axial velocity profile along the centerline for different Reynold numbers and the severity of stenosis. The axial velocity has the same pattern and magnitude in the first part of the inlet, then the occurrence of the stenosis has changed the profile. The velocity profile for TYPE I is nearly consistent with the velocity of 1.5 along the longitudinal direction. However, as the radii of the occluded region became narrow, the velocity profiles started to increase in magnitude at the onset of the stenosis and emerged along the axial occluded centerline. Then, the movement of the blood reduces gradually to zero as reaching the apex of the bifurcation artery. Figure 12 presents the radial velocity profile along the axial position, $x = 1.45$ and $x = 1.55$ with different Reynold numbers and heights of stenosis (A1 and A2), respectively. Comparing Figure 12 and Figure 10, we observe that the velocity exhibited in axial velocity is greater compared to the radial velocity although it might vary in sign.

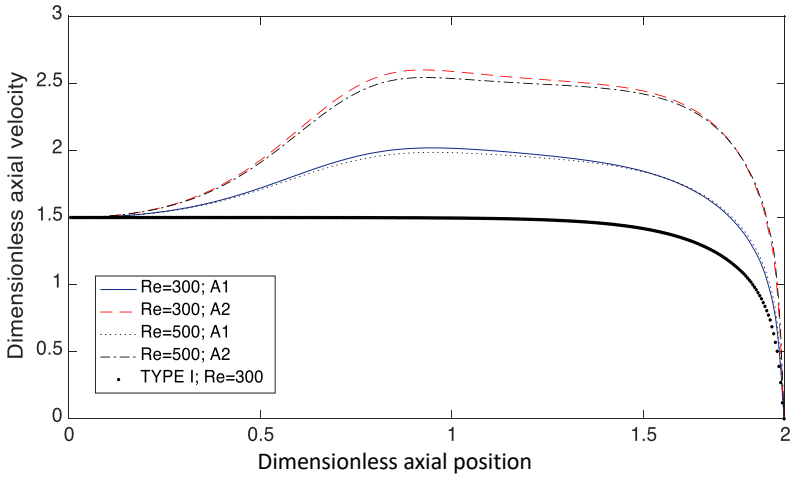

Fig. 11. Velocity profile at centreline of artery along the longitudinal direction with different Reynold number and maximum height of stenosis

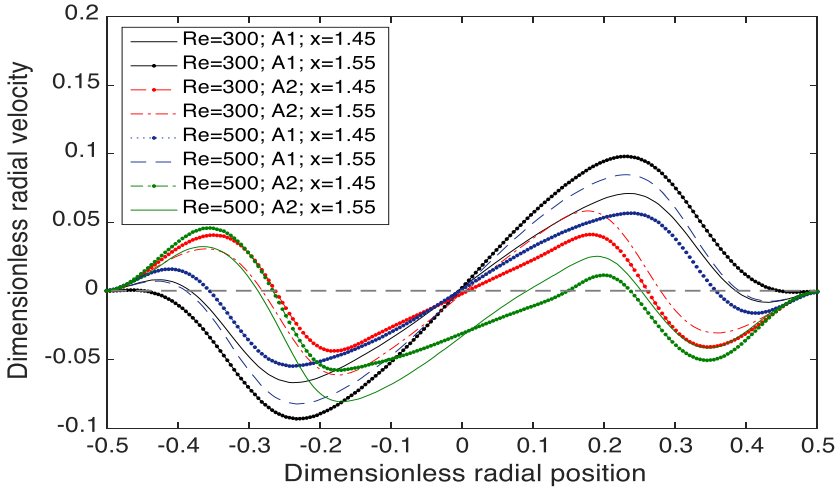

Fig. 12. Radial velocity profile at different location with different Reynold number and maximum height of stenosis

Figures 13 (a) – 13 (d) shows the cross-sectional profiles of the axial velocity of TYPE III corresponding to different axial positions in the bifurcated artery with different degrees of occlusion stenosis, and Reynold number, (Re = 300 and Re=500). The velocity at the location of $x = 0.85$ is zero on both sides of the wall due to the assumption of the non-slip rigid vessel. All the profiles except for the TYPE I, are skewed to the left to the outer wall of the mother artery. The flow is much faster at the upper vessel wall. In addition, the profile is significantly increased as the occlusion area increase. The velocity profile is flattened by the Reynolds number due to the dominant fluid inertia force.

Figure 13 (b) shows the velocity profile at $x = 1.55$ for TYPE III, which is located right after the stenosis at the outer of the lower wall of the mother artery. The magnitude of the axial velocity is dependent on the Reynold number and occlusion degrees. The healthier artery with no plaque accumulation gives a lower axial velocity profile. The velocity of the blood flow with stenosis A2 is higher as compared to the flow with stenosis A1. The reversal flow and separation have been detected at the upper vessel wall (see Figure 13 (b)) due to the sudden change in the arterial radii. Figures 13 (c) – 13 (d) show the cross-sectional axial velocity profiles at $x = 3.05$ and $x = 3.15$ of the daughter artery, respectively. A negative velocity value implies the backflow is formed at $x = 3.05$

for stenosis severity of A2. At $x = 3.15$, the magnitude of the negative velocity is lesser and the maximum point of the velocity is skewed to the right to the outer wall of the bifurcated artery.

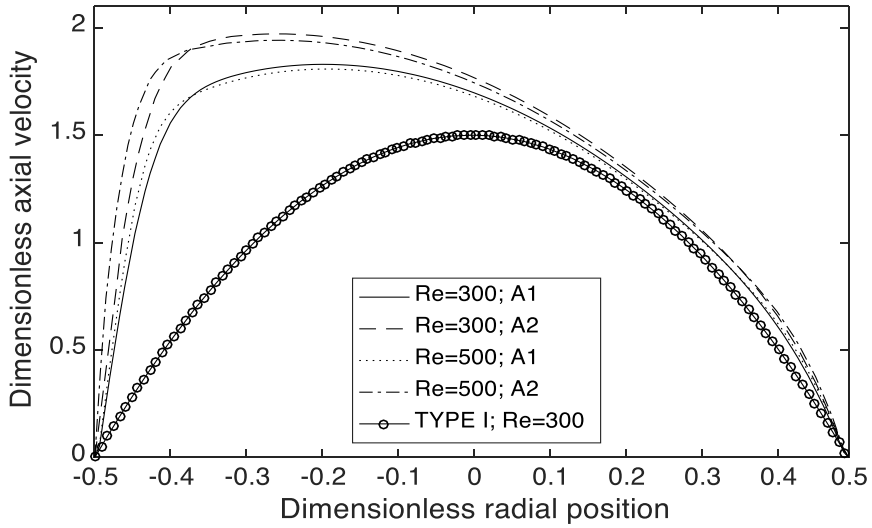

(a) TYPE III at $x = 0.85$

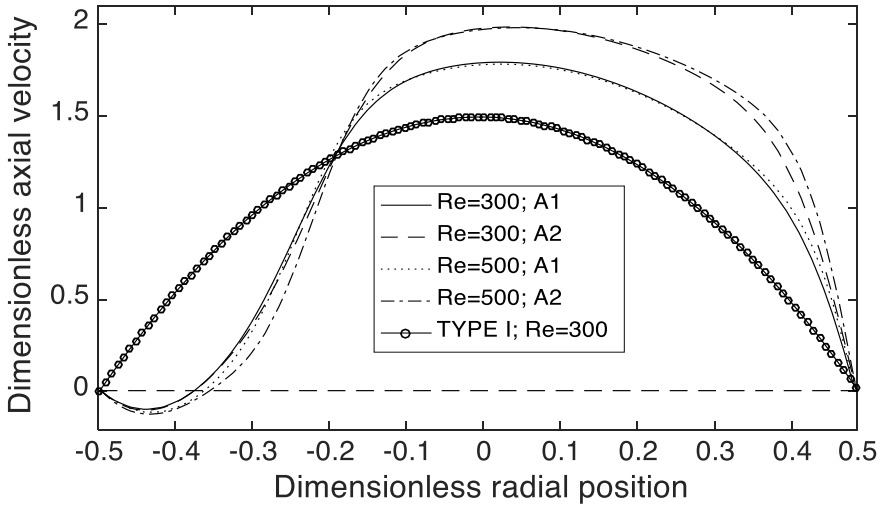

(b) TYPE III at $x = 1.55$

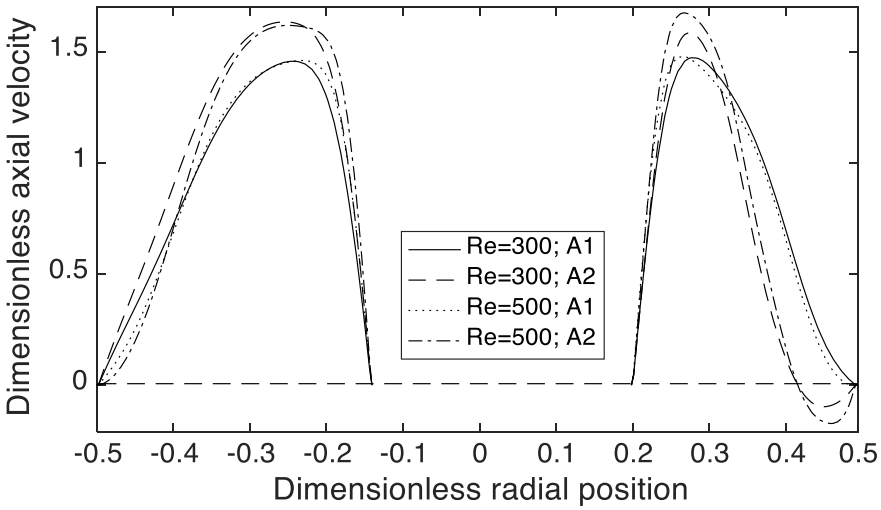

(c) TYPE III at $x = 3.05$

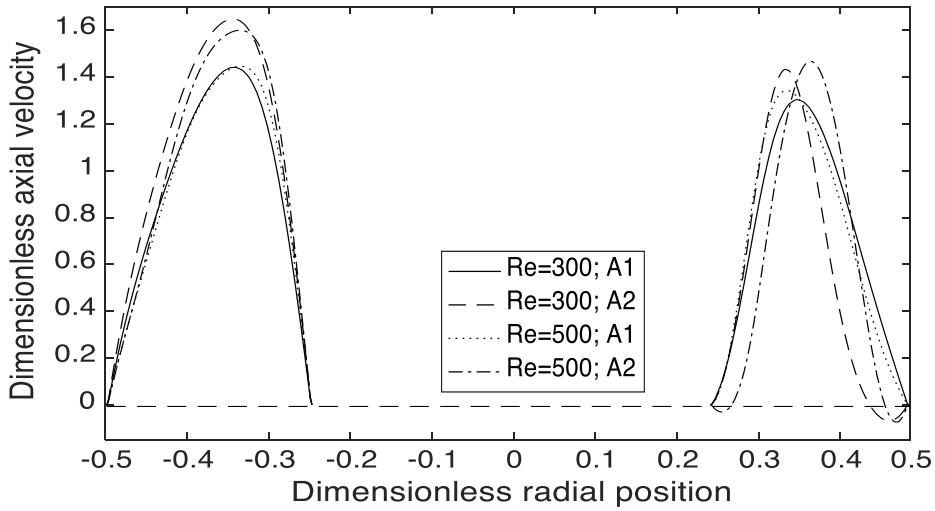

(d) TYPE III at $x = 3.15$

Fig. 13. Velocity profile TYPE III with different Reynold number (300 and 500), and maximum height of stenosis, (A1 and A2)

Figures 14 (a) – 14 (c) demonstrates the cross-sectional profiles of the axial velocity corresponding to different axial positions in the bifurcated artery for the different maximum height of stenosis (A1 and A2), and Reynold number (Re = 300 and Re=500). The velocity at locations of *x*=2, 3, and 3.5 with occlusion of A2 is highest compared to A1. Furthermore, the fluid with Reynold number 300 has a significantly highest velocity magnitude than 500. The flow divider or apex at the location of *x*=2 has dropped the velocity profile as seen in Figure 14 (a). Then the fluid flow is divided into the upper and lower part due to the bifurcate of the artery as shown in Figures 14 (b) and 14 (c) at the location of *x*=3 and *x*=3.5 respectively. The stenosis has decelerated the flow of blood inside the bifurcated artery. Thus, the velocity profiles are reduced as the fluid passes from *x*=3 to x=3.5 (see Figures 14 (b) and 14 (c)).

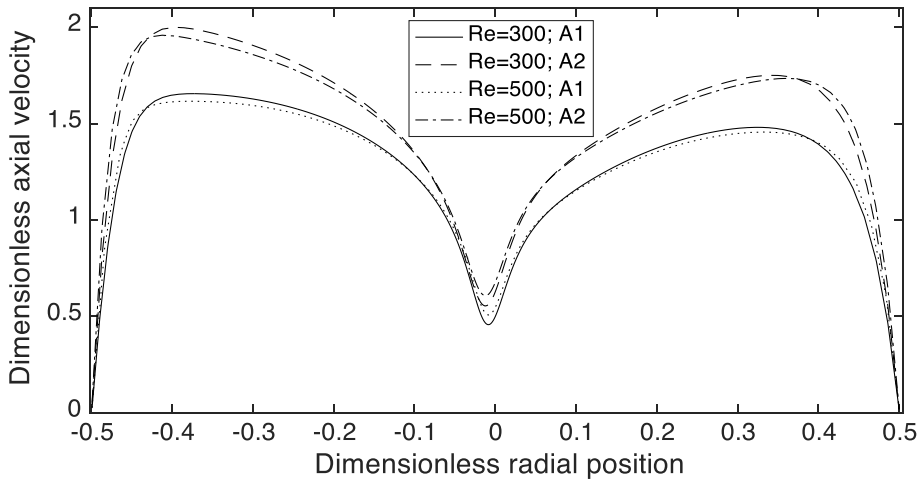

(a) TYPE IV at $x = 2$

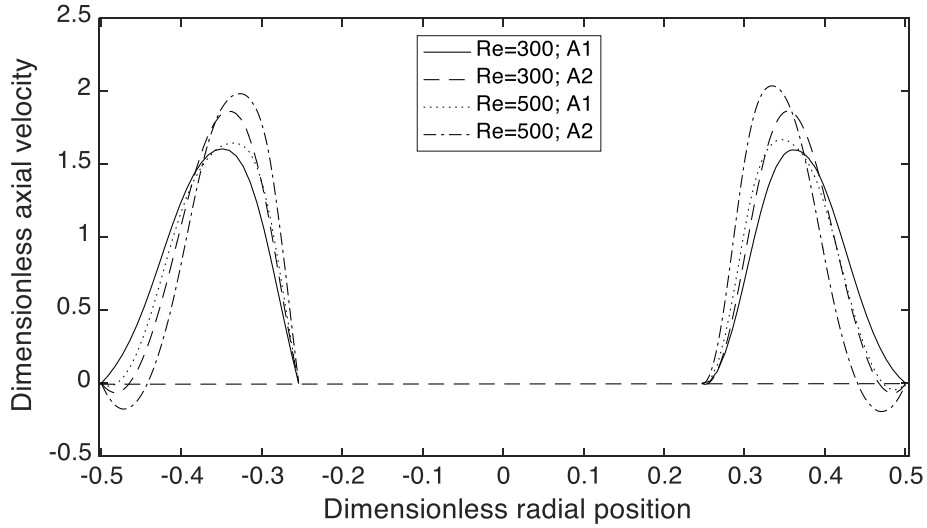

(b) TYPE IV at $x = 3.0$

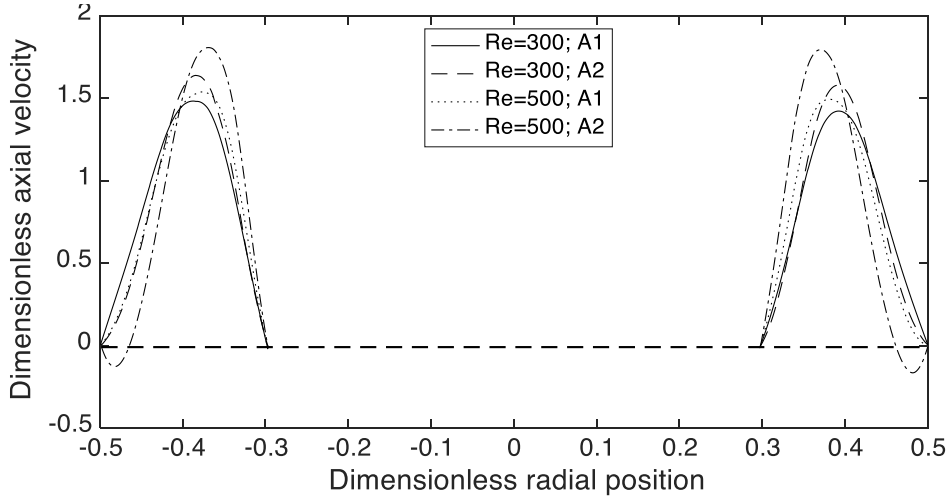

(c) TYPE IV at $x = 3.5$

Fig. 14. Velocity profile for TYPE IV with different Reynold number (300 and 500), and maximum height of stenosis, (A1 and A2)

6. Conclusions

The effects of bioheat transfer on the behaviour of blood flow through a bifurcated channel without and with different type of stenosis are presented. In this study, new results presented which have not been published before, specifically effects of maximum height of stenosis and Reynolds number on the velocity of streaming bloods are discussed graphically. The results reveal that the maximum velocity increases as the degrees of constriction increase, and lower Reynolds number enhances the axial velocity at the central axis of an artery. Overall, velocity profiles for all TYPE's of model, significantly affected by the location of stenosis and the profiles were depicted based on at the evaluated location. The maximum velocity highest in bifurcate throat compare to the throat at mother artery which may contributed by the narrowing and small range of artery radius. TYPE IV shows the highest value of maximum velocity compare others TYPE's (TYPE II and TYPE III) due to less severe which allows the flow less decelerate as passthrough the flow divider. Despite that, the curves of negative value imply that the backflow is formed. The flow reversal that is developed in the post-

stenotic region near the outer wall surface has influenced the surrounding blood flow by pushing it toward the inner wall of the daughter branch. In conclusion, the results presented agree well with physical observations and provide and insight into the connection between atherosclerosis, stenosis and the pattern of bioheat transfer. As suggestion for further study, more details explanation on the characteristics of blood flow such as wall pressure, wall shear stress, the streamlines patterns, temperature profiles, as well as Nusselt number of streaming bloods will needed to be discuss graphically.

Acknowledgement
This work was funded by the Ministry of Higher Education under FRGS, Registration Proposal No: FRGS/1/2019/STG06/UTM/02/21 and Research Management Centre, Universiti Teknologi Malaysia (UTM) under UTM Fundamental Research (UTMFR) grant 21H48.

References

[1] Zain, Norliza Mohd, and Zuhaila Ismail. "Modelling of Newtonian blood flow through a bifurcated artery with the presence of an overlapping stenosis." *Malaysian Journal of Fundamental and Applied Sciences* 13, no. 2017 (2017): 304-309. https://doi.org/10.11113/mjfas.v13n4-1.866

[2] Singh, A. K. "Effects of shape parameter and length of stenosis on blood flow through improved generalized artery with multiple stenoses." *Advances in Applied Mathematical Biosciences* 3, no. 1 (2012): 41-48.

[3] Ledesma, Jessica M., Daniel N. Riahi, and Ranadhir Roy. "Two-phase flow in a catheterized artery with atherosclerosis." *Journal of Theoretical and Applied Mechanics* 51, no. 2 (2013): 409-418.

[4] Riahi, D. N.; Garcia, A. E. Blood Flow in an Artery with Multi Stenosis. *Mathematics and Computers in Biology and Biomedical Informatics*, 2014, 45–48.

[5] Iakovou, Ioannis, Lei Ge, and Antonio Colombo. "Contemporary stent treatment of coronary bifurcations." *Journal of the American College of Cardiology* 46, no. 8 (2005): 1446-1455. https://doi.org/10.1016/j.jacc.2005.05.080

[6] Varshney, Gaurav, V. K. Katiyar, and Sushil Kumar. "Numerical modeling of pulsatile flow of blood through a stenosed tapered artery under periodic body acceleration." *Journal of Mechanics in Medicine and Biology* 10, no. 02 (2010): 251-272. https://doi.org/10.1142/S0219519410003393

[7] Pedley, Timothy J., and Y. C. Fung. "The fluid mechanics of large blood vessels." (1980). https://doi.org/10.1017/CBO9780511896996

[8] Alimohamadi, Haleh, Mohsen Imani, and Behjat Forouzandeh. "Computational analysis of transient non-Newtonian blood flow in magnetic targeting drug delivery in stenosed carotid bifurcation artery." *International Journal of Fluid Mechanics Research* 42, no. 2 (2015). https://doi.org/10.1615/InterJFluidMechRes.v42.i2.50

[9] Bose, Sayan, and Moloy Banerjee. "Magnetic particle capture for biomagnetic fluid flow in stenosed aortic bifurcation considering particle–fluid coupling." *Journal of Magnetism and Magnetic Materials* 385 (2015): 32-46. https://doi.org/10.1016/j.jmmm.2015.02.060

[10] Zarins, Christopher K., Don P. Giddens, B. K. Bharadvaj, Vikrom S. Sottiurai, Robert F. Mabon, and Seymour Glagov. "Carotid bifurcation atherosclerosis. Quantitative correlation of plaque localization with flow velocity profiles and wall shear stress." *Circulation research* 53, no. 4 (1983): 502-514. https://doi.org/10.1161/01.RES.53.4.502

[11] Srinivasacharya, Darbhasayanam, and Gade Madhava Rao. "Micropolar fluid flow through a stenosed bifurcated artery." *Nonlinear Analysis: Modelling and Control* 22, no. 2 (2017): 147-159. https://doi.org/10.15388/NA.2017.2.1

[12] Zain, Norliza Mohd, and Zuhaila Ismail. "Hartmann and Reynolds Numbers Effects in the Newtonian Blood Flow of a Bifurcated Artery with an Overlapping Stenosis." *MATEMATIKA: Malaysian Journal of Industrial and Applied Mathematics* (2019): 213-227. https://doi.org/10.11113/matematika.v35.n2.1177

[13] Basri, Adi Azriff, Shah Mohammed Abdul Khader, Cherian Johny, Raghuvir Pai, Muhammad Zuber, Kamarul Arifin Ahmad, and Zanuldin Ahmad. "Numerical Study of Haemodynamics Behaviour in Normal and Single Stenosed Renal Artery using Fluid–Structure Interaction." *Journal of Advanced Research in Fluid Mechanics and Thermal Sciences* 51, no. 1 (2018): 91-98.

[14] Jamali, Muhammad Sabaruddin Ahmad, and Zuhaila Ismail. "Simulation of Heat Transfer on blood flow through a stenosed bifurcated artery." *Journal of Advanced Research in Fluid Mechanics and Thermal Sciences* 60, no. 2 (2019): 310-323

[15] Hegde, Pranav, SM Abdul Khader, Raghuvir Pai, Masaaki Tamagawa, Ravindra Prabhu, Nitesh Kumar, and Kamarul Arifin Ahmad. "CFD Analysis on Effect of Angulation in A Healthy Abdominal Aorta-Renal Artery Junction." *Journal*

of Advanced Research in Fluid Mechanics and Thermal Sciences 88, no. 1 (2021): 149-165. https://doi.org/10.37934/arfmts.88.1.149165

[16] Ramdan, Salman Aslam, Mohammad Rasidi Rasani, Thinesh Subramaniam, Ahmad Sobri Muda, Ahmad Fazli Abdul Aziz, Tuan Mohammad Yusoff Shah Tuan Ya, Hazim Moria, Mohd Faizal Mat Tahir, and Mohd Zaki Nuawi. "Blood Flow Acoustics in Carotid Artery." *Journal of Advanced Research in Fluid Mechanics and Thermal Sciences* 94, no. 1 (2022): 28-44. https://doi.org/10.37934/arfmts.94.1.2844

[17] Ningappa, Abhilash Hebbandi, Suraj Patil, Gowrava Shenoy Belur, Augustine Benjamin Valerian Barboza, Nitesh Kumar, Raghuvir Pai Ballambat, Adi Azriff Basri, Shah Mohammed Abdul Khader, and Masaaki Tamagawa. "Influence of Altered Pressures on Flow Dynamics in Carotid Bifurcation System Using Numerical Methods." *Journal of Advanced Research in Fluid Mechanics and Thermal Sciences* 97, no. 1 (2022): 47-61. https://doi.org/10.37934/arfmts.97.1.4761

[18] Rabby, Mir Golam, Sumaia Parveen Shupti, and Md Molla. "Pulsatile non-newtonian laminar blood flows through arterial double stenoses." *Journal of Fluids* 2014 (2014). https://doi.org/10.1155/2014/757902

[19] Friedman, Morton H., Vivian O'Brien, and Louis W. Ehrlich. "Calculations of pulsatile flow through a branch: implications for the hemodynamics of atherogenesis." *Circulation Research* 36, no. 2 (1975): 277-285. https://doi.org/10.1161/01.RES.36.2.277

[20] Ogulu, A., and Tamunoimi M. Abbey. "Simulation of heat transfer on an oscillatory blood flow in an indented porous artery." *International communications in heat and mass transfer* 32, no. 7 (2005): 983-989. https://doi.org/10.1016/j.icheatmasstransfer.2004.08.028

[21] Li, Jiangye, and Hulin Huang. "Effect of magnetic field on blood flow and heat transfer through a stenosed artery." In *2010 3rd International Conference on Biomedical Engineering and Informatics*, vol. 5, pp. 2028-2032. IEEE, 2010. https://doi.org/10.1109/BMEI.2010.5639654

[22] Srikanth, D., JV Ramana Reddy, Shubha Jain, and Anup Kale. "Unsteady polar fluid model of blood flow through tapered ω-shape stenosed artery: Effects of catheter and velocity slip." *Ain Shams Engineering Journal* 6, no. 3 (2015): 1093-1104. https://doi.org/10.1016/j.asej.2015.01.003

[23] Zaman, A., N. Ali, O. Anwar Bég, and M. Sajid. "Heat and mass transfer to blood flowing through a tapered overlapping stenosed artery." *International Journal of Heat and Mass Transfer* 95 (2016): 1084-1095. https://doi.org/10.1016/j.ijheatmasstransfer.2015.12.073

[24] Majee, Sreeparna, and G. C. Shit. "Numerical investigation of MHD flow of blood and heat transfer in a stenosed arterial segment." *Journal of Magnetism and Magnetic Materials* 424 (2017): 137-147. https://doi.org/10.1016/j.jmmm.2016.10.028

[25] Bessonov, Nikolay, Adélia Sequeira, Sergey Simakov, Yu Vassilevskii, and Vitaly Volpert. "Methods of blood flow modelling." *Mathematical modelling of natural phenomena* 11, no. 1 (2016): 1-25. https://doi.org/10.1051/mmnp/201611101

[26] Chakravarty, S., and P. K. Mandal. "Mathematical modelling of blood flow through an overlapping arterial stenosis." *Mathematical and computer modelling* 19, no. 1 (1994): 59-70. https://doi.org/10.1016/0895-7177(94)90116-3

[27] Ismail, Zuhaila, Ilyani Abdullah, Norzieha Mustapha, and Norsarahaida Amin. "A power-law model of blood flow through a tapered overlapping stenosed artery." *Applied Mathematics and Computation* 195, no. 2 (2008): 669-680. https://doi.org/10.1016/j.amc.2007.05.014

[28] Abdullah, Ilyani, and Norsarahaida Amin. "A micropolar fluid model of blood flow through a tapered artery with a stenosis." Mathematical Methods in the Applied Sciences 33, no. 16 (2010): 1910-1923. https://doi.org/10.1002/mma.1303

[29] Bakheet, Ahmed, Esam A. Alnussaiyri, Zuhaila Ismail, and Norsarahaida Amin. "Blood flow through an inclined stenosed artery." *Applied Mathematical Sciences* 10, no. 5 (2016): 235-254. https://doi.org/10.12988/ams.2016.511701

[30] Ismail, Zuhaila, Ilyani Abdullah, Norzieha Mustapha, and Norsarahaida Amin. "A power-law model of blood flow through a tapered overlapping stenosed artery." *Applied Mathematics and Computation* 195, no. 2 (2008): 669-680. https://doi.org/10.1016/j.amc.2007.05.014

[31] Misra, J. C., and B. Pal. "A mathematical model for the study of the pulsatile flow of blood under an externally imposed body acceleration." *Mathematical and Computer Modelling* 29, no. 1 (1999): 89-106. https://doi.org/10.1016/S0895-7177(98)00180-0

[32] Clough, Ray W. "The finite element method in plane stress analysis." In *Proceedings of 2nd ASCE Conference on Electronic Computation, Pittsburgh Pa., Sept. 8 and 9, 1960*. 1960.

[33] Weddell, Jared C., JaeHyuk Kwack, P. I. Imoukhuede, and Arif Masud. "Hemodynamic analysis in an idealized artery tree: differences in wall shear stress between Newtonian and non-Newtonian blood models." *PloS one* 10, no. 4 (2015): e0124575. https://doi.org/10.1371/journal.pone.0124575

[34] YASHKUN, UBAIDULLAH, SYED FEROZ SHAH, ASIF ALI SHAIKH, and MS CHANDIO. "BLOOD FLOW SIMULATION IN CAROTID ARTERY BIFURCATION USING FINITE ELEMENT METHOD." *Sindh University Research Journal-SURJ (Science Series)* 45, no. 3 (2013).

[35] Achaba, Louiza, Mohamed Mahfouda, and Salah Benhadida. "Numerical study of the non-Newtonian blood flow in a stenosed artery using two rheological models." *Thermal Science* 20, no. 2 (2016): 449-460. https://doi.org/10.2298/TSCI130227161A